

Copyright notice:

Copyright 2019 Society of Photo-Optical Instrumentation Engineers and Optical Society of America. One print or electronic copy may be made for personal use only. Systematic reproduction and distribution, duplication of any material in this paper for a fee or for commercial purposes, or modification of the content of the paper are prohibited.

This is an author prepared version of a published paper

Reference and link to the official online version:

P. Strenge, B. Lange, C. Grill, W. Draxinger, M. M. Bonsanto, C. Hagel, R. Huber, R. Brinkmann, "Segmented OCT data set for depth resolved brain tumor detection validated by histological analysis," Proc. SPIE 11228, Optical Coherence Tomography and Coherence Domain Optical Methods in Biomedicine XXIV, 112282O (21 February 2020);
doi: 10.1117/12.2545659

Segmented OCT data set for depth resolved brain tumor detection validated by histological analysis

P. Strenge^a, B. Lange^a, C. Grill^b, W. Draxinger^b, M. M. Bonsanto^c, C. Hagel^d, R. Huber^b, R. Brinkmann^{a,b}

^aMedical Laser Center Lübeck, Peter-Monnik-Weg 4, 23562 Lübeck, Germany;

^bInstitute of Biomedical Optics, University of Lübeck, Peter-Monnik-Weg 4, 23562 Lübeck, Germany;

^cDepartment of Neurosurgery, University Medical Center Schleswig-Holstein, Campus Lübeck, Ratzeburger Allee 160, 23562 Lübeck, Germany;

^dInstitute for Neuropathology, University Medical Center Hamburg-Eppendorf, Martinistraße 52, 20251 Hamburg, Germany

ABSTRACT

The aim of this work is the creation of segmented data set consisting of optical coherence tomography (OCT) scans, which were taken of brain tumor tissue with different tumor infiltration rates. In an ongoing clinical study more than 140 human brain samples with different infiltration grades were recorded *ex vivo* with two OCT systems, a spectral domain OCT system and a swept-source OCT system that uses a 1310 nm Fourier domain mode locked laser. The histological analysis of the recorded samples builds the ground truth for labeling the corresponding OCT B-Scans. The segmented data set gained from this process will be used to train a classification algorithm, taking into account structural and optical properties such as the attenuation coefficient. In the future the classification algorithm together with a microscope integrated OCT system will be used for the *in vivo* identification of brain tumors as a guidance tool for the surgeon to increase tumor resection efficiency.

Keywords: Optical coherence tomography, OCT, FDML laser, MHz-OCT, brain tumor, brain imaging, neurosurgery

1. INTRODUCTION

In Germany approximately 43,000 new oncological cases of disease in the central nervous system are diagnosed every year. For the majority of patients the microsurgical tumor resection is a therapeutic option. The extent of this resection and the tumor histology correlate with the survival expectation, especially in glioma surgery [1]. However, the detection of residual tumor during neurosurgery remains an important challenge: There is a low inherent contrast between malignant tissue and the healthy tissue during the resection. Some tumors such as glioblastoma, are highly invasive and lack a true histological border to the normal brain tissue [1]. Prior work has shown that OCT has the potential to detect brain tumors by evaluating optical properties compared to healthy brain tissue [2-5]. Based on these findings, en face maps can be created for the surgical guidance during tumor resection with the disadvantage that the depth information gained through OCT is lost [3].

The aim of this work is to preserve the depth information through a labeled OCT dataset, which allows the depth resolved tissue classification based on the attenuation coefficient and structural features [6]. The labeled OCT dataset was created by locally analyzing histological sections from different brain tissue samples and detecting correlations between the OCT scan and the histological sections.

2. MATERIALS AND METHODS

2.1 Data Acquisition

For the data acquisition of *ex vivo* malign brain tissue two OCT systems were used: 1. A spectral domain (SD) OCT system (Callisto by Thorlabs GmbH, Dachau Germany) with an imaging wavelength 930 nm, a lateral resolution of 8

μm and axial resolution of $7 \mu\text{m}$. A Fourier domain mode locked MHz-OCT system (OMES by Optores GmbH, München Germany) with an imaging wavelength at 1310 nm , lateral resolution of $30 \mu\text{m}$ and axial resolution of $15 \mu\text{m}$. During the resection of 20 malign brain tumors (mostly glioblastoma multiforme) on average 8 samples per tumor were extracted by a neurosurgeon with a Yasargil forceps. The samples were taken from the main tumor tissue itself as well as the tumor borders to healthy tissue. The samples of the tumor borders were taken after the tumor resection was defined as a complete resection by the neurosurgeon based on the intraoperative white light and the fluorescence information from the surgical microscope. Each sample was placed into an agar cuboid prior to the imaging, which fixed the position of the sample and gave the sample a certain shape, which eased the creation of H&E histological sections and the later structural classification (see Figure 1). The sample size varied from 9 to 75 mm^3 . The imaging of each prepared tissue sample with the two OCT systems was performed within 15 minutes after the extraction by the neurosurgeon. Additionally during the scanning with the SD-OCT a spectator camera acquired an en face image.

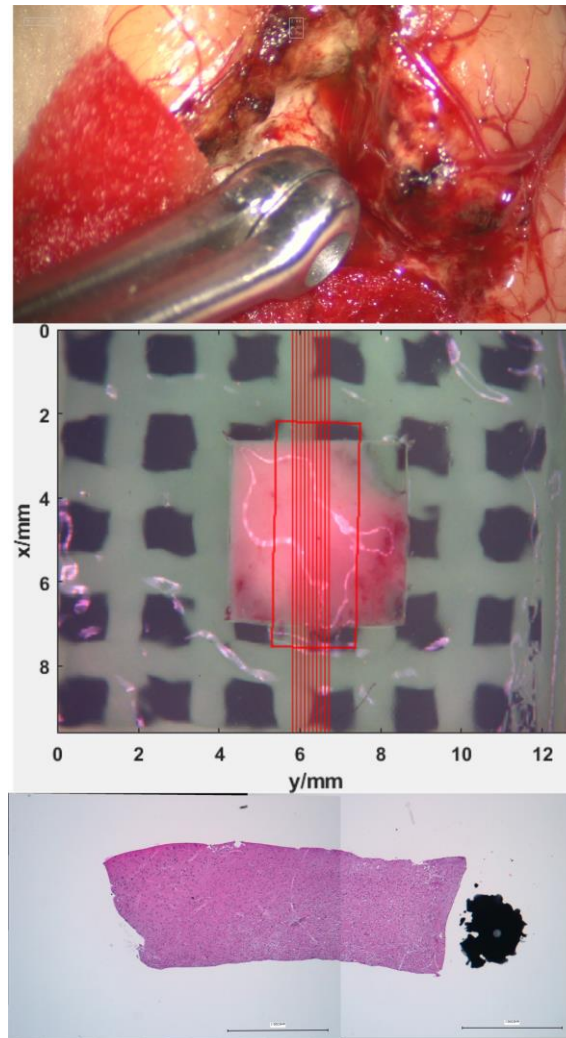


Figure 1 Extraction of a tissue sample with a Yasargil forceps (top). Brain sample during *ex vivo* scanning (red rectangle is field of view of the Thorlabs Callisto OCT, 10 red stripes represent the positions where the sample was cut, middle). Example of an H&E stained histological section from the sample above (bottom)

After the imaging each sample was fixated with 4.5% formalin in order to stop the tissue decay and was sent to the neuropathology for tissue staining and histological analysis. 10 H&E stained histological sections were then created from each sample. The sample was cut according to individual cutting instructions, which were based on the red cutting lines on camera en face image (see Figure 1). The distance between each cut was 0.1 mm and the orientation was the same as

in the acquired B-scans. The histological sections were then segmented by a neuropathologist, who used the following labels: White matter (0%, 0-30%, 30-60%, >60% tumor infiltration), grey matter (0%, 0-30%, 30-60%, >60% tumor infiltration), vessel, necrosis, coagulation, edema, cyst, bleeding and connective tissue. The result of the data acquisition per extracted tissue sample were 1 C-scan for each of the two OCT systems, an en face camera image and 10 labeled H&E stained histological sections.

2.2 Registration of the Datasets

The OCT C-scans were registered onto the en face camera image in order to be able to find the corresponding B-scans to the histological sections. This step allows the transfer of the label, which were set by the neuropathologist, from the histological sections onto the corresponding OCT B-scans. The registrations were achieved through a landmark based affine approach of the en face projections of the C-scans on to the en face camera image. The en face projections of the C-scans $I(x,y)$ were calculated through the mean intensity projection along the depth axis z of the C-scan $V(x,y,z)$.

$$I(x, y) = \frac{1}{N_z} \sum_{z=1}^{N_z} V(x, y, z) \quad (1)$$

Figure 2 shows an example of the en face projection calculated from the C-scans of the two OCT systems.

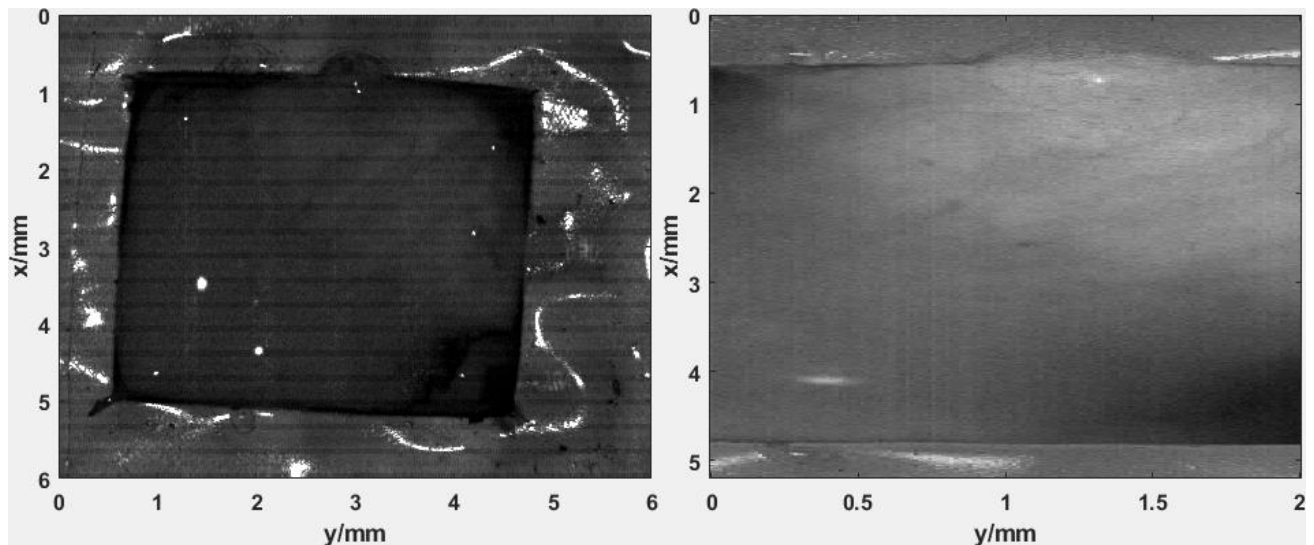


Figure 2 En face projections of the C-scans acquired by the MHz-OCT system (left) and the SD-OCT system (right).

The landmark based affine approach was used, because the images vary in rotation, translation, scaling and modality. The former makes it much more difficult to find corresponding features automatically, which is why the landmarks were manually set. An affine transformation between two point clouds can be described through the following equation [7]:

$$\mathbf{p}_2 = \mathbf{A}\mathbf{p}_1 = \begin{pmatrix} A_{11} & A_{12} & A_{13} \\ A_{21} & A_{22} & A_{23} \\ 0 & 0 & 1 \end{pmatrix} \mathbf{p}_1 \quad (2)$$

\mathbf{p}_1 and \mathbf{p}_2 are the two point clouds, which contain N points. The points are represented through the coordinates $(x_{i,n}, y_{i,n}, 1)^T$ and \mathbf{A} is the affine transformation matrix. In order to calculate the transformation, the calculations for x and y component of \mathbf{p}_2 are separated. The x component can be determined by the following equation:

$$x_{2,n} = (A_{11} \quad A_{12} \quad A_{13}) \begin{pmatrix} x_{1,n} \\ y_{1,n} \\ 1 \end{pmatrix} = x_{1,n}A_{11} + y_{1,n}A_{12} + A_{13} \quad (3)$$

In order to solve this equation for the components of \mathbf{A} , a least squares approach was chosen. This approach minimizes the error $E(A_{11}, A_{12}, A_{13})$ calculated through the sum of squared differences:

$$E(A_{11}, A_{12}, A_{13}) = \sum_{n=1}^N (x_{2,n} - (x_{1,n}A_{11} + y_{1,n}A_{12} + A_{13}))^2 \quad (4)$$

The spatial derivatives of Eq. 4 were calculated for the determination of the minimum of the error E , which results in the following system of equations:

$$\begin{pmatrix} \sum_1^N x_{2,n}x_{1,n} \\ \sum_1^N x_{2,n}y_{1,n} \\ \sum_1^N x_{2,n} \end{pmatrix} = \begin{pmatrix} \sum_1^N x_{1,n}^2 & \sum_1^N x_{1,n}y_{1,n} & \sum_1^N x_{1,n} \\ \sum_1^N x_{1,n}y_{1,n} & \sum_1^N y_{1,n}^2 & \sum_1^N y_{1,n} \\ \sum_1^N x_{1,n} & \sum_1^N y_{1,n} & N \end{pmatrix} \begin{pmatrix} A_{11} \\ A_{12} \\ A_{13} \end{pmatrix} \quad (5)$$

This system of equations can now be solved for the components of \mathbf{A} . The same steps can be carried out for the y component of \mathbf{p}_2 , which leads to the following systems of equation:

$$\begin{pmatrix} \sum_1^N y_{2,n}x_{1,n} \\ \sum_1^N y_{2,n}y_{1,n} \\ \sum_1^N y_{2,n} \end{pmatrix} = \begin{pmatrix} \sum_1^N x_{1,n}^2 & \sum_1^N x_{1,n}y_{1,n} & \sum_1^N x_{1,n} \\ \sum_1^N x_{1,n}y_{1,n} & \sum_1^N y_{1,n}^2 & \sum_1^N y_{1,n} \\ \sum_1^N x_{1,n} & \sum_1^N y_{1,n} & N \end{pmatrix} \begin{pmatrix} A_{21} \\ A_{22} \\ A_{23} \end{pmatrix} \quad (6)$$

Since the camera image had the largest FOV, it was used as a reference and the en face images of the OCT systems were registered onto that image. This allowed the determination of the transformation between the two OCT C-scans later on. The en face camera image is acquired through an off the shelf software (Thorimage by Thorlabs GmbH), which imprints the FOV of the SD-OCT onto the camera image as a red rectangle (see Figure 1). The first step to calculate the transformation matrix \mathbf{A}_1 , which represents the affine transformation from the SD OCT enface image to the camera en face image, is the detection of the corner points of the red rectangle in the camera image. These points are then registered on the corner points of the SD-OCT en face image. The transformation matrix \mathbf{A}_2 , which describes the affine transformation from the MHZ-OCT en face image onto the camera image, was calculated with manually set points on both images. The affine transformation from the SD-OCT to the MHZ-OCT can be determined by the following equation:

$$\mathbf{A}_3 = \mathbf{A}_1(\mathbf{A}_2)^{-1} \quad (7)$$

3. RESULTS

Since the position of the histological section in the original sample is roughly known through the cutting lines on the camera image (see Figure 1), the affine transformations between the en face images were determined. It is now possible to transform the cutting lines from the camera en face image on to the en face images of the SD-OCT and the MHZ-OCT, which is shown in Figure 3.

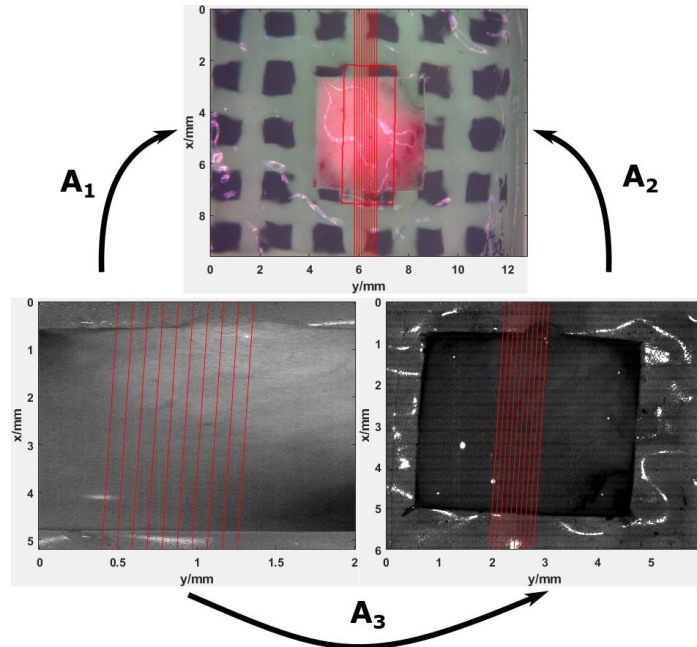


Figure 3 Transformation of the cutting lines from the camera en face image (top) on to the en face projections of the two OCT systems (SD-OCT in the bottom left, MHZ-OCT in the bottom right).

This step enabled the extraction of B-scans from the two OCT datasets, which correspond to the histological sections defined by the cutting lines (see Figure 4 and Figure 5).

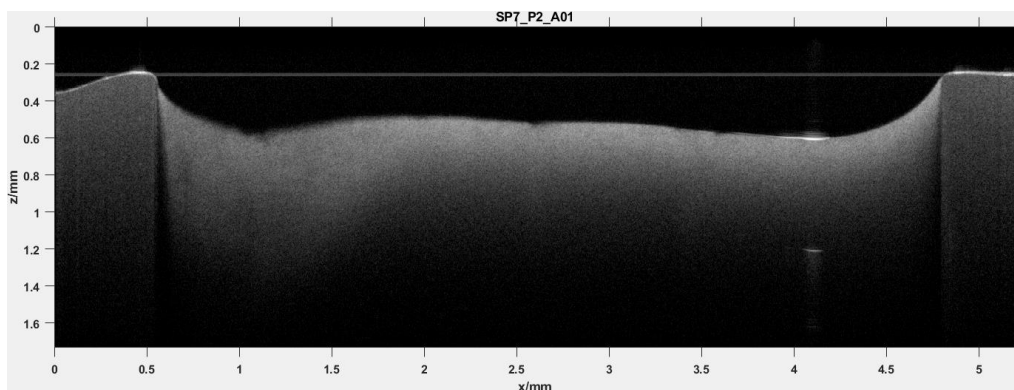


Figure 4 B-scan representing the first cutting line extracted from the SD-OCT C-scan.

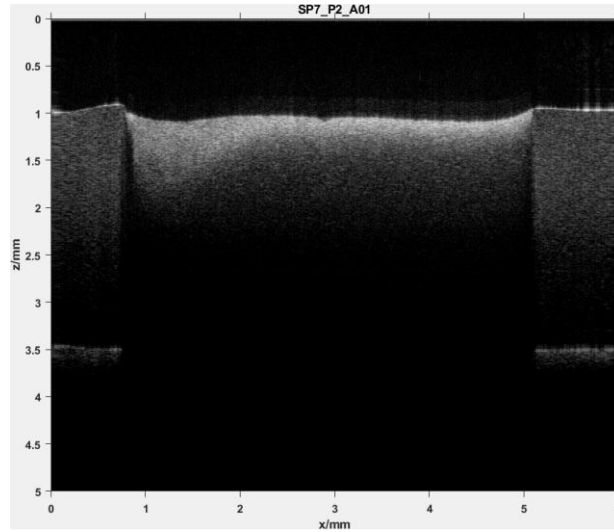


Figure 5 B-scan representing the first cutting line extracted from the MHZ-OCT C-scan.

After extracting the corresponding B-scans, the labels set by the neuropathologist are now manually transferred from the histological section onto the B-scans, in order to create the desired data sets for the classification. Figure 6 shows one result of this process for the B-scan of the SD-OCT. It is important to note, that only regions, which can be identified with a high certainty, were segmented in the B-scan. Transitions zones are hard to identify and a false segmentation would ruin the classification results later on.

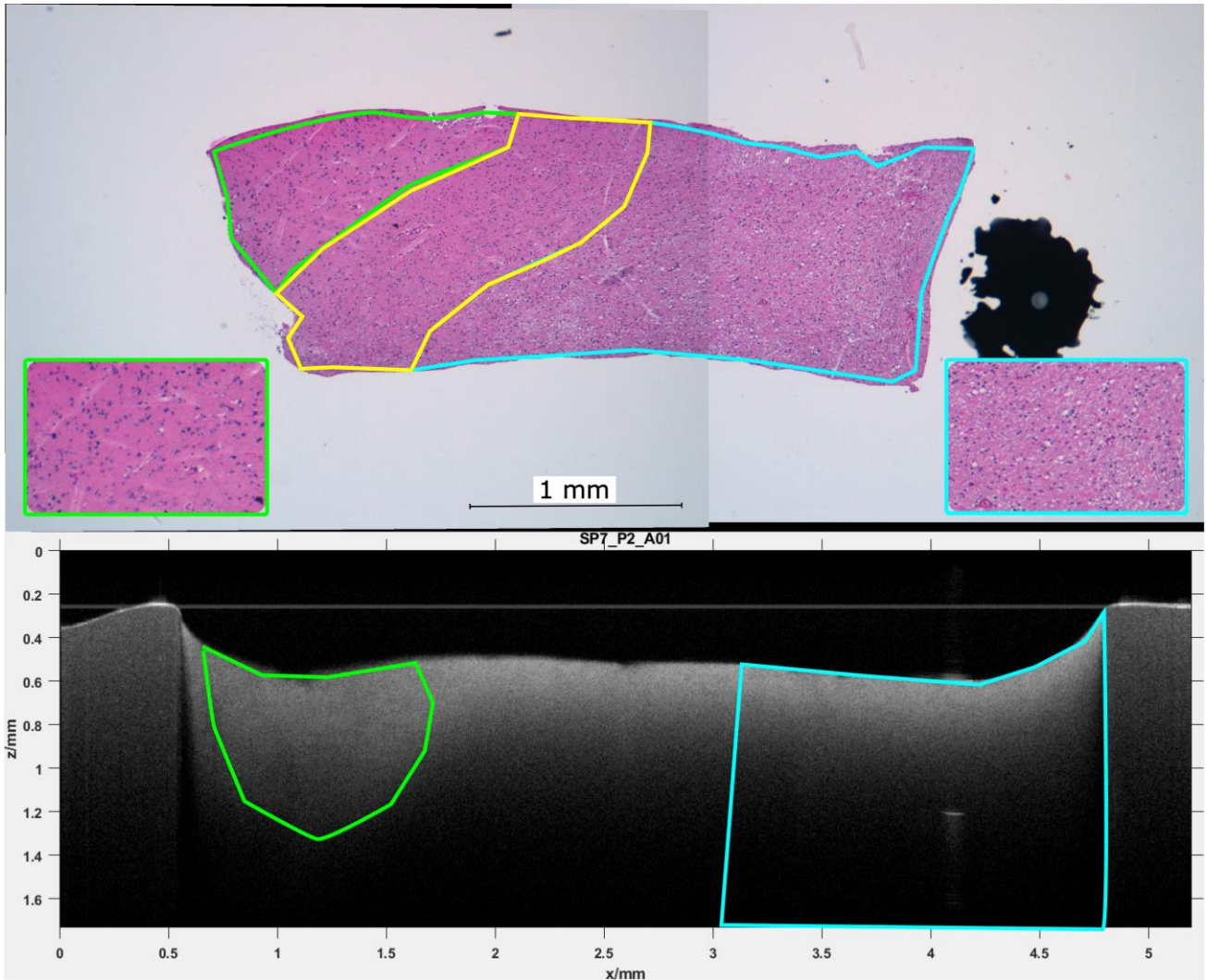


Figure 6 First histological section of the sample from Figure 1, segmented by the neuropathologist (top): grey matter (green), white matter with edema (blue), transition zone (yellow). Corresponding B-scan from the SD-OCT C-scan with transferred labels (bottom).

4. OUTLOOK AND DISCUSSION

It was shown, that it is possible to create a labeled dataset of OCT B-scans. At the moment not all the data was put through this process, since the labeling of the histological section takes a lot of time. In the end the data set will consist of up to 2500 segmented OCT B-scans with 15 different labels. The method of transferring the labels from the histological sections on to the OCT B-scans must be developed further, since the manual approach is very time consuming and is prone to human error. The implementation of an automatic label transferring program on the other hand is very difficult, because the scale and the surface structure of the samples sometimes change during the transport and preparation process for the creation of the histological sections. The gained labeled OCT dataset will be used in the future as a ground truth for depth resolved supervised classification algorithms in order to detect the different tumor infiltration zones. Intensity based, structural analysis and optical properties will be used for the classification.

ACKNOWLEDGMENT

This research is funded by the Federal Ministry of Education and Research Grants No.: 13GW0227A, 13GW0227B 13GW0227C and the European Union project ENCOMOLE-2i (Horizon 2020, ERC CoG no. 646669). Evaluation of human brain tissue was approved by Ethics committee of University Medical Center Schleswig-Holstein, Campus Lübeck, Germany, No.: 18-204.

REFERENCES

- [1] A. Giese, R. Bjerkvig, M. E. Berens et al., "Cost of migration: invasion of malignant gliomas and implications for treatment," *J Clin Oncol*, 21(8), 1624-36 (2003).
- [2] A. Giese, H. Böhringer, J. Leppert *et al.*, "Non-invasive intraoperative optical coherence tomography of the resection cavity during surgery of intrinsic brain tumors." *Photonic Therapeutics and Diagnostics II* 6078, 60782Z, International Society for Optics and Photonics (2006).
- [3] C. Kut, K. L. Chaichana, J. Xi et al., "Detection of human brain cancer infiltration ex vivo and in vivo using quantitative optical coherence tomography," *Sci Transl Med*, 7(292), 292ra100 (2015).
- [4] M. Lenz, R. Krug, C. Dillmann et al., "Automated differentiation between meningioma and healthy brain tissue based on optical coherence tomography ex vivo images using texture features," *J Biomed Opt*, 23(7), 1-7 (2018).
- [5] K. Yashin, M. Karabut, V. Fedoseeva *et al.*, "Multimodal optical coherence tomography in visualization of brain tissue structure at glioblastoma (experimental study)," *Современные технологии в медицине*, 8(1 (eng)), (2016).
- [6] K. A. Vermeer, J. Mo, J. J. Weda *et al.*, "Depth-resolved model-based reconstruction of attenuation coefficients in optical coherence tomography," *Biomed Opt Express*, 5(1), 322-37 (2013).
- [7] A. Ardehshir Goshtasby *et al.*, "Image Registration - Principles, Tools and Methods," Springer Science & Business Media, (2012)